06,08

# Microdomain structures investigation in LNOI thin films of different thickness using an AFM tip

© Ya.V. Bodnarchuk, R.V. Gainutdinov

National Research Center „Kurchatov Institute“,
Moscow, Russia

E-mail: deuten@mail.ru

Received November 26, 2025
Revised February 17, 2026
Accepted February 17, 2026

The results of domain recording and evolution using an AFM tip were obtained for three film thickness: 300 nm, 500 nm, 700 nm. It was shown that domain growth and formation depend significantly on the thickness of the thin filmś waveguide layer. At minimum recording voltages, stable and regular domains are recorded in waveguides with thicknesses of 300 and 500 nm, but this regularity and stability are not observed in a thin film of 700 nm with the same recording parameters Domain coalescence has been studied, which depends both on the recording period between domains and on the thickness of the thin film.

**Keywords:** domain structure, thin film, atomic force microscopy, lithium niobate.

DOI: 10.61011/PSS.2026.02.63385.8822

## 1. Introduction

Thin films of lithium niobate ($LiNbO_3$-on-Insulator, LNOI) has gained a growing attracted in today's integral photonics and microelectronics due to their unique piezoelectric, nonlinear-optical and ferroelectric properties [1–4]. Domain structures in thin films are of particular interest for controlling the nonlinear processes, providing efficient the nonlinear optical-frequency conversion in the quasi-phase matching (QPM) mode [5], paving the way for miniaturization of devices and increasing their efficiency.

Among the promising methods of nanodomain engineering in thin films of LNOI are the atomic force microscopy, electron and ion irradiation [10–12]. These are the invasive, non-contact and non-destructive methods with the possibility of obtaining structures with a period up to a submicron scale. These non-contact methods allow preventing the negative edge effects peculiar to the ferroelectrics at the electrode boundary, which are observed when using a common field method for creating regular domain structures (RDS) by applying an external field to a system of electrodes deposited on the crystal surface. The advantage of these methods, directly related to this study, is the possibility of creating RDS on the polar surfaces of a LNOI thin film. This geometry may be applicable for some waveguide optical circuits. The purpose of this work is to study the dynamics of domains in thin films of different thicknesses and to identify their common features and differences, which will make it possible to create regular domain structures in LNOI.

## 2. Experimental procedure

Thin single-crystal layers of LNOI ($LiNbO_3$-on-Insulator) having polar (Z-) orientation (Nanoln Electronics, Jinan, China) were used in the experiment.

Thin films of LNOI were fabricated using the method of ion implantation with light ions (H, He, etc.) followed by cleavage of a thin single-crystal layer of lithium niobate $LiNbO_3$ and the subsequent fixing of the thin film to the substrate (in our case, the thin film is a sandwich structure consisting of a stripped off thin single-crystal layer of $LiNbO_3$, a conductive Au/Pt layer and $SiO_2$ layer, which is fixed on a substrate of a bulk crystal of $LiNbO_3$). Thin films and waveguides fabrication methods are described in detail in papers [13–16].

LNOI, schematically shown in Figure 1, is composed of a thin single-crystal wafer of $LiNbO_3$ and $LiNbO_3$ crystal of Z-cut separated by the layers of $SiO_2$ and metal. The waveguide effect in the upper (thin) wafer is reached due to the ratio $n_{\text{SO}} < n_{\text{LN}}$ (where $n_{\text{SO}}$ and $n_{\text{LN}}$ — refractive indices $SiO_2$ and $LiNbO_3$ respectively). In the studied samples the thickness of the waveguide layer $LiNbO_3$ was 700 nm, 500 and 300 nm, thickness of metallic layer Au/Pt — 100 nm and thickness of $SiO_2$ — 1.905 $\mu$m. The samples had the following geometry $\text{X} \times \text{Y} \times \text{Z} = 10 \times 10 \times 0.5$ mm (see Figure 1, block-diagram).

The domain structures of various configurations were fabricated by microscopic methods of scanning and vector lithography using an atomic force microscope (AFM) [17]. The experiments were carried out using probe laboratory Ntegra Prima SPM(NT−MDT, Moscow). The vector lithography method was implemented using a graphical template made with variable recording intervals by applying $U_{DC}$ between a conductive probe (with Pt coating) in contact with a polar (Z-) surface. One-dimensional (1D) and two-dimensional (2D) domain structures were recorded by applying a constant field $U_{DC}$ of AFM probe in LNOI film and are schematically shown in Figure 1. The domain originated at the point of the probe-surface contact grows

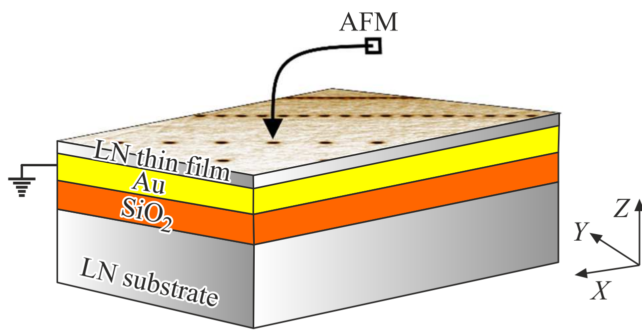


**Figure 1.** Scheme of recording domains with an AFM probe in an LNOI thin film of polar (Z-) orientation.

axially along Z axis. The recorded structures were studied by piezoresponse force microscopy (PFM) method. The exposure characteristics of the formation of single domains were measured. The local hysteresis loops of $H_\omega - U_{DC}$ ($H_\omega$ — signal of electromechanical response, $U_{DC}$ — AFM probe voltage) were measured using PFM-microscopy. Special attention was paid to the analysis of piezoelectric hysteresis loops that were used to determine the coercive voltage and bias voltage. A model of a flat capacitor was used to calculate the electric field.

## 3. Results

### 3.1. Piezoelectric hysteresis loops

Figure 2, *a* illustrates the hysteresis loops at $t_p = 100$ ms ($t_p$ — voltage pulse time) for the three different film thicknesses. All loops were measured at closely spaced points on thin films of different thicknesses. Figure 2, *b* shows piezoelectric hysteresis loops measured in a 500 nm thick thin film at $t_p = 70-1000$ ms.

The measured hysteresis loops qualitatively characterize the remaining polarization $P_{\text{rem}}$ and the coercive voltage $U_c$. From Figures 2, *a* and 2, *b*, it can be seen that there is a slight decrease in $E_c$, but this decrease is within the error range, so the loops can be considered as frequency-independent. This result is consistent with the data on classical lithium niobate $LiNbO_3$. The loops are unipolar, which may be the reason for the presence of a lower locking layer immediately following the waveguide layer. It can be seen from the data in Figure 2, *b* that the value $H_\omega$ does not depend on $t_p$ and there is no relaxation of the recorded domain structures, as a result of which no reverse switching occurs.

Figure 3 shows distribution of the coercive voltage $U_C$ versus the film thickness. From Figure 3 we see that coercive voltage, found from the hysteresis piezoelectric loops for LNOI 700 nm thick thin film is practically 2 times higher that for the 300 nm thick thin film.

A model of a flat capacitor was used to calculate the coercive field:

$$E = U/D,$$

where $D$ — thickness of the waveguide layer.

The model of a flat capacitor is in good agreement with the thin film data, and the numerical values for the coercive field are in good agreement with the coercive field of a congruent $LiNbO_3$ $E_c = 220$ kV/cm.

The table shows that for thin films with a thickness of 500 and 700 nm, as the pulse duration increases, the coercive field and the bias field decline, which is typical for classical ferroelectrics. In a 300 nm thick thin film, the coercive field does not change or increases slightly with increasing pulse, which may cause the impact of the lower locking layer or the film thickness itself during the domain recording.

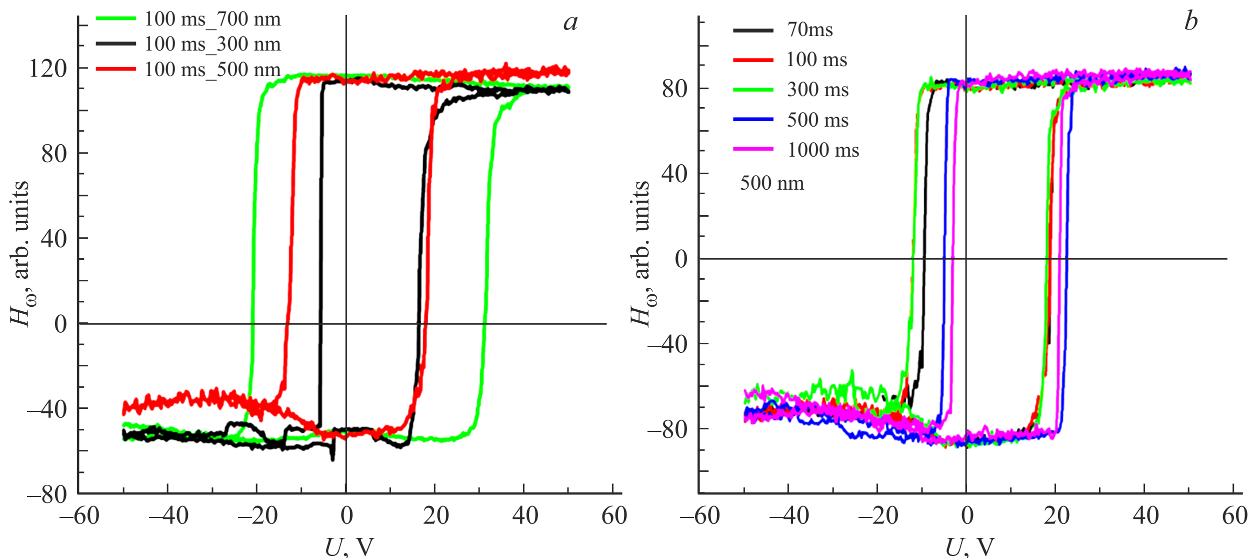


**Figure 2.** *a* — piezoelectric hysteresis loops in LNOI thin films measured for $t_p = 100$ ms; *b* — piezoelectric hysteresis loops in 500 nm thick LNOI thin films measured for $t_p = (70-1000)$ ms.

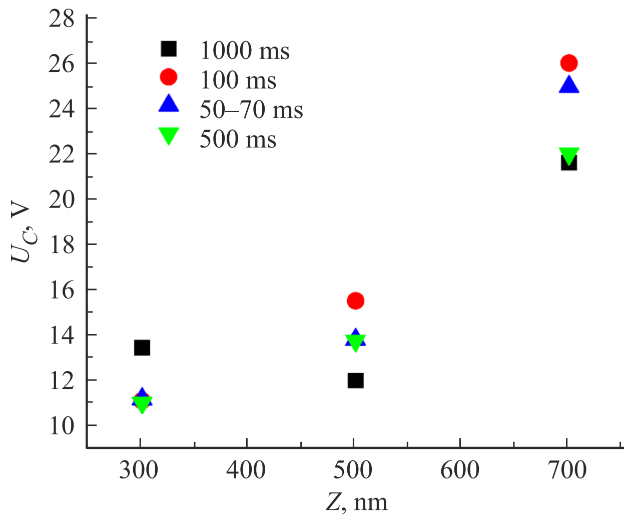


**Figure 3.** Distribution of the coercive voltage $U_C$ versus the film thickness.

Calculation of the coercive field $E_c$ for thin films using the flat capacitor model

| | $d = 300$ nm | $d = 500$ nm | $d = 700$ nm |
|---|---|---|---|
| $t_p = 100$ ms | 370 kV/cm | 310 kV/cm | 370 kV/cm |
| $t_p = 200$ ms | 367 kV/cm | 297 kV/cm | 333 kV/cm |
| $t_p = 500$ ms | 365 kV/cm | 275 kV/cm | 315 kV/cm |

### 3.2. Domains generated by AFM probe field

Figure 4 illustrates the PFM-image of registered domains at the exposure time of $t_p = 1000$ ms and voltage of $U_{DC} = 30$ V in thin films 300 (*a*), 500 (*b*) and 700 nm (*c*). The domains were recorded using a graphical template with a specific period in each row: $\Lambda = 1\,\mu$m, 500 nm, 200 nm and 100 nm, respectively. Based on PFM-image data we may see a difference in the regularity and reproducibility of the recorded domain structures in a 700 nm thick thin film. Whereas for a thin film with a thickness of 300 nm (as well as in a film with a thickness of 500 nm), a clearly structured domain record is observed in terms of shape with sustained periods.

This discrepancy in the records of domain structures may be explained by the fact that domains in thin films with thicknesses of 300 and 500 nm emerge over the entire thickness of the film and are pinned on the conductive layer. Whereas for a 700 nm thin film, the contribution of the depolarization field $E_{\text{dep}}$ is more pronounced, and the recorded domains are near-surface and do not reach the lower conductive layer. These domains are less stable due to the fact that „head-to-head" or „tail-to-tail" domains are formed. Note that this record is typical for minimum (initial) and average voltages. Whereas at a maximum of 50 V, the domains emerge over the entire thickness of the film.

Figure 5 shows a PFM image of the recorded domains of a 300 nm thick film at exposure time of $t_p = 100$ ms and voltage $U_{DC} = 50$ V. This result in domain recording is already similar for three film thicknesses at maximum applied voltages. When the domains approach each other at a certain distance, the domains begin to stick together, and their coalescence occurs. Coalescence may result from the domain boundary shorting on the lower conductive layer (suppressing inter-domain electrostatic repulsion). But this question is still open for study, since closely spaced domains with charged walls shall repel each other. Here, the charge most likely drains on the short-circuited conductive domain walls with the lower electrode.

Figure 6 shows the domains diameter versus $U_{DC}$ with the exposure time of $t_p = 100$ ms (*a*) and 1000 ms (*b*) for the 300, 500 and 700 nm thick thin films. It can be seen from the graphs that the greatest variation in data is observed for films with a thickness of 700 nm and $t_p = 100$ ms, and these data are poorly approximated. The data for the remaining two films are well approximated by

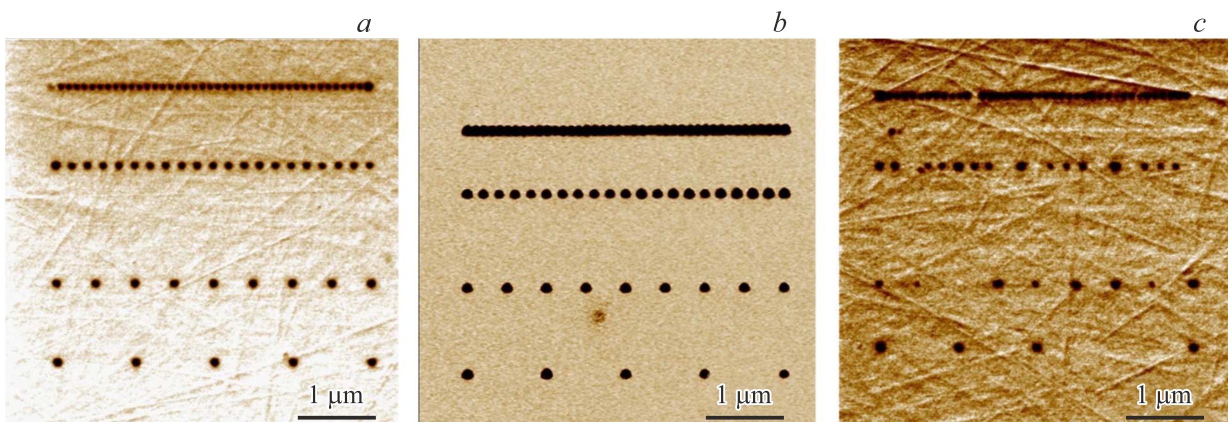


**Figure 4.** PFM-image of written domains at the exposure time of $t_p = 1000$ ms and voltage of $U_{DC} = 30$ V: *a* — film thickness 300 nm; *b* — film thickness 500 nm; *c* — film thickness 700 nm.

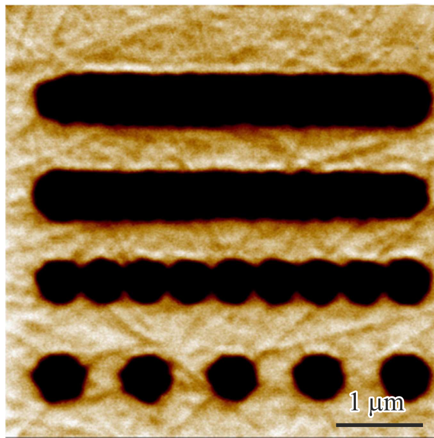


**Figure 5.** PFM-image of the recorded domains with the exposure time of $t_p = 100$ ms and voltage of $U_{DC} = 50$ V. The film thickness was 300 nm.

a linear function, which is consistent with the results of recording in congruent $LiNbO_3$.

Figure 6 shows that for a 300 nm thin film, the slope of $D(U_{DC})$ curve is greater, because the process of movement of the domain wall here occurs faster than in a 700 nm thick thin film.

Figure 7 shows the exposure dependences of the domain size on the recording time $D(t_p)$ for films with thicknesses of 300, 500, and 700 nm. The figure shows that for a film with a thickness of 700 nm, there is a greater spread of data than for thin films with a thickness of 300 and 500 nm. This is rather due to the fact that the domains in a 700 nm thick film lie near-surface and do not grow to the bottom locking layer. For films with thicknesses of 300 and 500 nm, the graph on the right shows a „saddle" of the domain growth, which may be caused by stopping of the domain wall motion.

The effect of the thin film thickness on recording and growth of domain structures is one of the main factors. It can be assumed that thin films with a thickness of 300 nm have a smaller size of the switched area in the volume, the electric field is more uniform across such a film, and the domain grows over its entire thickness and shorts on the bottom locking layer, as a result of which there is a complete switching, starting from the minimum voltages and times. At the same time, 700 nm thick films require long recording times to completely invert (switch) the domains.

## 4. Conclusion

In thin films LNOI ($LiNbO_3$ on-Insulator) of (Z-) orientation with a waveguide layer thickness of 300, 500 and 700 nm the stable 1D- and 2D-domain structures with a specific design were recorded using AFM probe and their properties were examined. The exposure dependences of $D(t_p)$ and $D(U_{DC})$ domains were calculated and analyzed. Based on the data on the kinetics of domain recording, a comparative analysis of the domain growth specifics within a thin film was performed. The results showed that thickness of the waveguide layer is a key factor influencing the stability and reproducibility of domains. It is shown that in the 700 nm thin films, there is a greater spread of data, which may be indicated by the fact that the domains do not emerge over the entire thickness of the film and are located near the surface or either a reverse switching occurs with shorter exposure times. Whereas for the 300 nm and 500 nm thick thin films the domains are of a „through" type and emerge across the entire film thickness. The obtained piezoelectric loops of hysteresis are unipolar. The value of $H_\omega$ does not depend on $t_p$, while there is no relaxation of

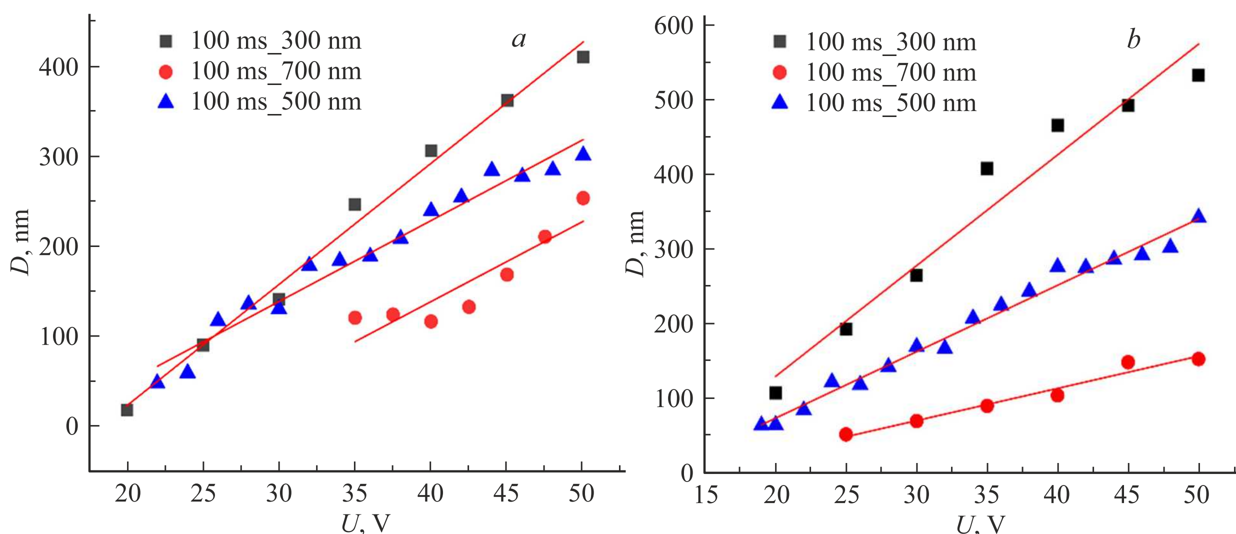


**Figure 6.** Diameter $D$ of domains versus $U_{DC}$ with the exposure time of $t_p = 100$ ms ($a$) and 1000 ms ($b$) for the 300, 500 and 700 nm thick thin films.

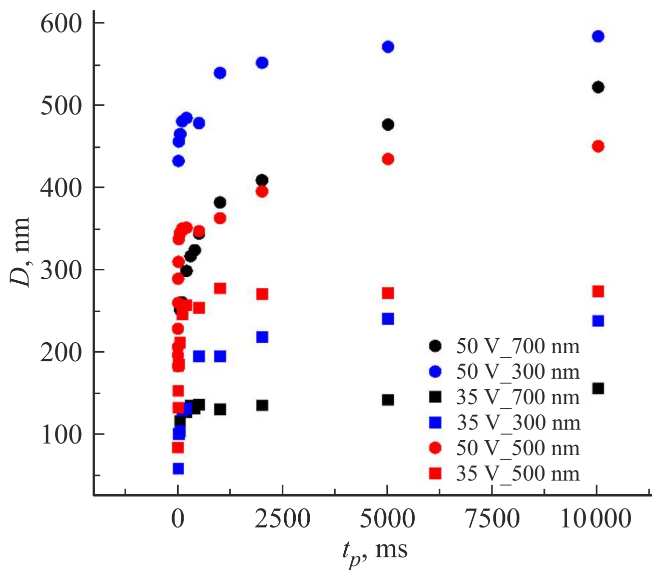


**Figure 7.** Exposure dependences of the domain size on the recording time $D(t_p)$ for the 300, 500 and 700 nm thick films.

the recorded domain structures, which indicates the absence of reverse switching. When the domains approach each other, coalescence occurs starting from a certain exposure time and voltage. Coalescence may result from the domain boundary shorting on the lower conductive layer (suppressing inter-domain electrostatic repulsion). These data are essential for engineering the stable domain structures, which are necessary, for example, in nonlinear optical frequency converters and devices based on periodic domain engineering.


## Funding

This study was carried out under the state assignment of the National Research Center „Kurchatov Institute".

## Acknowledgments

This study was carried out using the equipment of Shared Research Center „Structural diagnostics of materials" of the Kurchatov Complex Crystallography and Photonics NRC „Kurchatov institute".


## Conflict of interest

The authors declare that they have no conflict of interest.

## References


[1] T. Volk, M. Wöhlecke. Lithium niobate: defects, photorefraction and ferroelectric switching. Springer-Verlag, Berlin, Heidelberg (2008). 250 p.

[2] P. Ferraro, S. Grilli, P. De Natale. Ferroelectric Crystals for Photonic Applications, Including Nanoscale Fabrication and Characterization Techniques. Springer Series in Materials Science. (2009). 424 p.

[3] D. Sun, Y. Zhang, D. Wang, W. Song, X. Liu, J. Pang, D. Geng, Y. Sang, H. Liu. Light Sci. Appl. **9**, 197 (2020).

[4] J.J. Chakkoria, A. Dubey, A. Mitchell, A. Boes. Opto-Electron. Adv. **8**, 240139 (2025).

[5] A. Rao, S. Fathpour. IEEE J. Sel. Topics Quant. Electron., **24**, *6*, 4843–4855 (2018).

[6] R.V. Gainutdinov, T.R. Volk, H. Zhang. Appl. Phys. Lett. **107**, 162903 (2015).

[7] T.R. Volk, R.V. Gainutdinov, H. Zhang. Appl. Phys. Lett. **110**, 132905 (2017).

[8] T.R. Volk, R.V. Gainutdinov, H. Zhang. Crystals **7**, 137 (2017).

[9] R. Gainutdinov, T. Volk. Crystals **10**, 1160 (2020).

[10] I. Krasnokutska, J.L.J. Tambasco, A. Peruzzo. arXiv:2108.10839 (2021). doi.org/10.48550/arXiv.2108.10839

[11] B.N. Slautin, H. Zhu, V.Y. Shur. Ferroelectrics **576**, 119–128 (2021).

[12] B. Slautin, H. Zhu, V.Y. Shur. Ceram. Int. —bf47, 32900–32904 (2021).

[13] R. Huang, X. Zhang, M. Tang, R. Li, H. Xu, Y. Guo, Zh. Wang. Vacuum **227**, 113353 (2024).

[14] E. Lang, Th. Beechem, A. McDonald, T. Friedmann, R.H. Olsson, J.O. Stevens, B.G. Clark, K. Hattar. Thin Solid Films **768**, 139719 (2023).

[15] P.D. Townsend, P.J. Chandler, L. Zhang. Cambridge Univ. Press, Cambridge, UK. (1994). 296 p.

[16] F. Chen, X.L. Wang, K.M. Wang. Opt. Mat. **29**, 1523–1542 (2007).

[17] A.L. Kholkin, S.V. Kalinin, A. Roelofs, A. Gruverman. Scanning Probe Microscopy: Electrical and Electromechanical Phenomena at the Nanoscale. Springer-Verlag, N.Y. (2007). 310 p.


*Translated by T.Zorina*